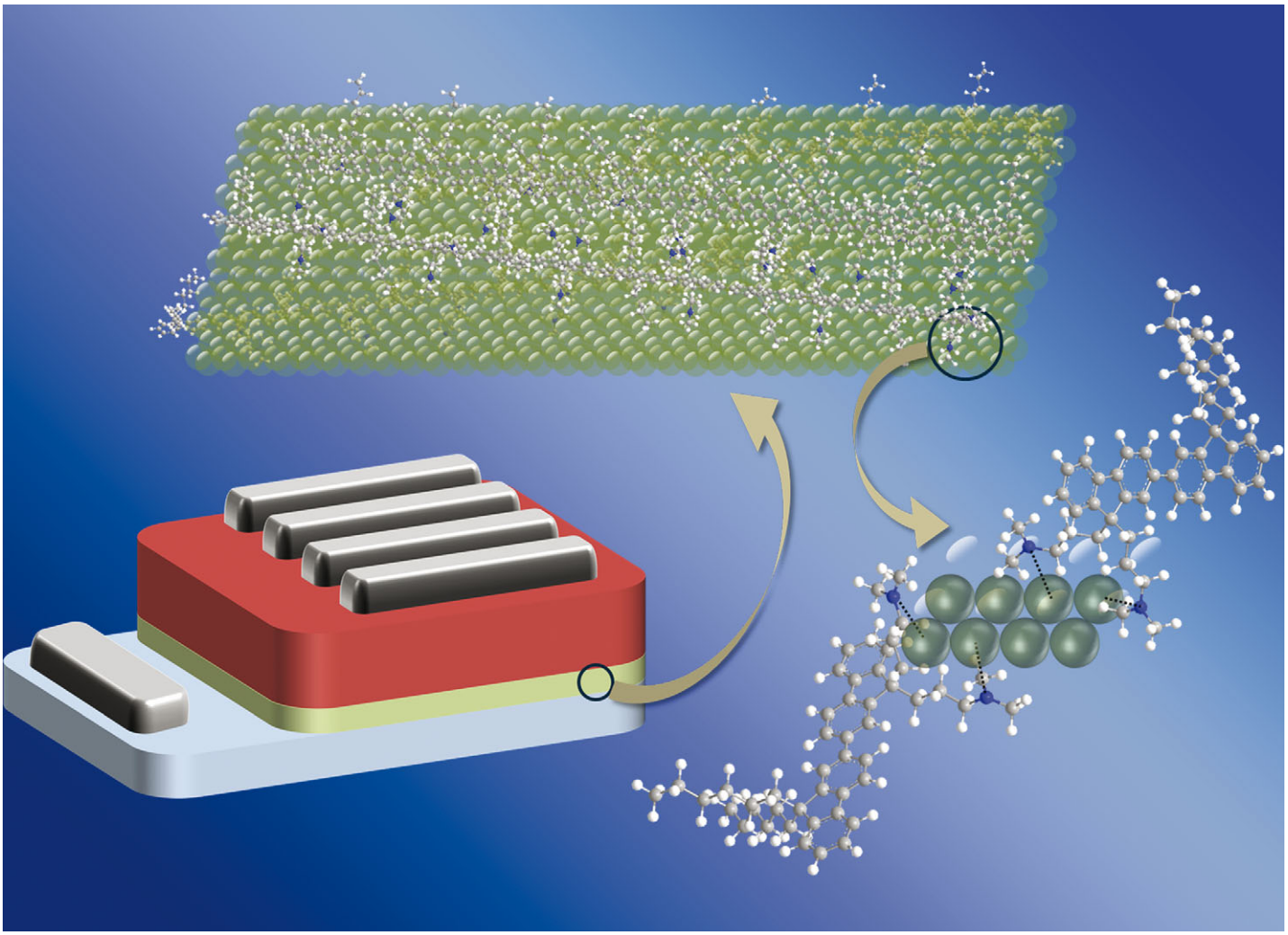

Showcasing research from the Nano and Information Materials Lab at Konkuk University, Seoul, Republic of Korea.

An organic–inorganic hybrid interlayer for improved electron extraction in inverted polymer solar cells

High-performance inverted polymer solar cells based on organic–inorganic hybrid ZnO–PFN electron extraction layer are constructed. Introducing PFN, which is a conjugated polymer, modifies the surface energy and energy levels of the electron extraction layer and enhances the electron mobility, PCE and long term stability of PSCs.

As featured in:

See Doo Kyung Moon *et al.*, *J. Mater. Chem. C*, 2016, **4**, 2463.

ROYAL SOCIETY OF CHEMISTRY

www.rsc.org/MaterialsC

Registered charity number: 207890

Journal of Materials Chemistry C

PAPER

View Article Online
View Journal | View Issue

Cite this: J. Mater. Chem. C, 2016, 4, 2463

An organic–inorganic hybrid interlayer for improved electron extraction in inverted polymer solar cells†

Eui Jin Lee,[a] Soo Won Heo,[b] Yong Woon Han[a] and Doo Kyung Moon*[a]

Received 11th November 2015,
Accepted 8th January 2016

DOI: 10.1039/c5tc03754a

www.rsc.org/MaterialsC

We fabricated inverted polymer solar cells (PSCs) using an organic–inorganic hybrid interlayer for electron extraction. The surface energy and surface defects of an organic–inorganic ZnO–PFN hybrid film, which was prepared by dissolving the conjugated polymer electrolyte poly[(9,9-bis(3′-(*N*,*N*-dimethylamino)propyl)-2,7-fluorene)-*alt*-2,7-(9,9-dioctyl-fluorene)] (PFN) in a ZnO solution, were reduced, compared to ZnO film. By introducing the ZnO–PFN electron extraction layer, the interfacial contact between the active and electron extraction layers was improved and the series resistance of the PSC device was decreased. As a result, electron extraction from the active layer to the electrode was enhanced. The highest power conversion efficiency (PCE) of the inverted PSCs was 9.2%. Moreover, the ZnO–PFN-based inverted PSCs showed improved long-term stability compared to ZnO-based devices. The ZnO–PFN interlayer aimed to overcome the drawbacks of the conventional hydrophilic surface of ZnO, based on the properties of the conjugated polymer (PFN) without the need for additional processes. It was therefore simple to fabricate the inverted PSCs, making the devices commercially viable.

Introduction

Bulk heterojunction (BHJ) polymeric solar cells (PSCs) have emerged as a new commercially viable source of energy due to their advantages of easy fabrication, low cost, flexibility and abundant availability.[1,2] However, the low power conversion efficiency (PCE) of BHJ PSCs remains one of the major obstacles, although recent advances in PSC-related research has shown 10% PCE through interfacial modifications such as introducing processing additives,[3–7] interlayers,[8–10] nanostructures,[2,11] solvent treatment[12,13] or modification of polymer design.[14] For a high PCE value, typical BHJ PSCs consist of a photoactive layer in which a donor material (polymer) is blended with an acceptor (fullerene derivative), and phase separation occurs in the mixture. The photoactive layer is placed between an indium tin oxide (ITO)/poly(3,4-ethylenedioxythiophene:polystyrene sulfonate) (PEDOT:PSS) anode and a low work function metal (such as Ca, Ba, or Al) cathode. In the conventional structure of a PSC, the hygroscopic and acidic PEDOT:PSS causes corrosion of the ITO electrode and degradation of the photoactive layer, undermining the long-term stability of the PSC. In addition, the top metal cathode is susceptible to oxidation because it is both air and water sensitive, deteriorating the efficiency of the PSC.[1,2,15] Low structural stability poses a limitation to the commercialization of BHJ PSCs.

To address the abovementioned problems, inverted structured PSCs have been actively developed. In an inverted structure, the top low work function metal electrode is replaced by a high work function metal (Au) anode to increase the hole collection efficiency. In addition, air stable, transparent metal oxides (such as ZnO, TiO_x, and ZMO) and conjugated polymer electrolytes (CPEs) are used as the electron-extracting interlayer.[1,2,16] The use of an electron extraction layer and air-stable metal electrodes instead of a hygroscopic PEDOT–PSS layer enables inverted PSCs to undergo self-encapsulation and provide longer ambient stability than conventional PSCs.[1,2,15,16] The efficiency of inverted PSCs is also boosted by vertical phase separation, which is induced by a surface energy difference between the donor polymer and the fullerene derivative.[6,11,17] In other words, phase separation occurs in polymer-based bulk heterojunction films upon spin coating, constructing an upper layer with a low surface energy polymer and a lower layer with a fullerene derivative. This phenomenon restricts charge transport in a conventional device.[18,19] However, in an inverted structure, the irradiation is reversed by ITO as the cathode, and the charge transport is improved and balanced as a result. Cao *et al.*[15] and Ouyang *et al.*[20] used a modified ITO cathode as a means of controlling the energy level of the cathode.

[a] Department of Materials Chemistry and Engineering, Konkuk University, 1 Hwayang-dong, Gwangjin-gu, Seoul 143-701, Republic of Korea. E-mail: dkmoon@konkuk.ac.kr
[b] RIKEN Center for Emergent Matter Science (CEMS) 2-1 Hirosawa, Wako, Saitama 351-0198, Japan

† Electronic supplementary information (ESI) available. See DOI: 10.1039/c5tc03754a

ZnO is commonly used as a buffer layer because of its environmental stability, high electron mobility and optical transparency.[1,2,11] However, ZnO is a hydrophilic inorganic material and makes poor interfacial contact with the hydrophobic organic photoactive layer, resulting in charge trapping in a surface of the inorganic material.[1,21,22] For improved extraction of electrons in inverted PSCs, modification of the interface between the electrode and the organic photoactive layer is regarded as an important issue. The interface between a cathode and an organic photoactive layer can be modified to enhance the electron extraction efficiency by introducing an organic interlayer between the ZnO and photoactive layers,[19,23,24] forming a fullerene derivative layer on the ZnO layer,[21,25–27] or introducing a nanostructured ZnO layer.[11,28,29]

Chang *et al.* reported an increased PCE (from 7.28% to 8.01%) in inverted devices using ZnO/CPE as an electron extraction layer, wherein poly[(9,9-bis(3′-(*N*,*N*-dimethylamino)propyl)-2,7-fluorene)-*alt*-2,7-(9,9-dioctyl-fluorene)] (PFN) and poly[3-(6-trimethylammoniumhexyl) thiophene] (PTMAHT) were used as the polymer CPEs.[19] Yang *et al.* also used a ZnO/PFN double layer and improved the PCE of inverted devices from 6.1% to 8.4%.[24] However, in those studies, modifying the interface of the electron extraction layer meant an additional process for a finished ZnO layer, complicating the entire process.

In this study, we dissolved PFN, which is well known as an electron transporting/collecting layer for polymer emitting diodes and PSCs,[10,30] in a ZnO solution and deposited an organic–inorganic ZnO–PFN hybrid film as a single layer for electron extraction. The surface structure of the ZnO–PFN film was characterized by contact angle measurements, XPS and UPS analysis. To determine the effects of the ZnO–PFN interlayer, the surface energy, energy level and electron mobility were investigated. We fabricated inverted PSCs using the ZnO–PFN hybrid material as a cathode modifier. As a result, the PSCs, which were fabricated in this study, have the potential to be a cost-effective way to harness solar energy due to their simple structure and process. More importantly, the PCE of PSC efficiency was as high as 9.2%, and the long-term stability was improved compared with a ZnO-based device.

Experimental section

Preparation of ZnO solution

The ZnO solution was synthesized according to previously published procedures.[1,2] A gram of zinc acetate dehydrate ($C_4H_6O_4Zn{\cdot}2(H_2O)$ 99.5%, Aldrich) and 0.28 g of monoethanolamine ($HOCH_2CH_2NH_2$, 98%, Aldrich, 1 : 1 mol ratio) were dissolved into 10 ml of 2-methoxyethanol ($CH_3OC_2H_4OH$, 99.8%, Aldrich) and hydrolyzed for 12 hours. The ZnO–PFN thin film was prepared by dissolving 0.5–2 mg of PFN into the 1 ml of ZnO solution.

Inverted PSC fabrication

To fabricate the inverted PSC devices, patterned ITO glasses were washed by sonication in detergent, 2-propanol and deionized water in sequence. After cleaning, the ITO glasses were dried at 120 °C and UV-ozone-treated for 10 minutes. The ZnO solution and ZnO–PFN solution were separately spin-coated onto different ITO glasses and annealed at 150 °C in air to obtain an electronic transport layer (~10 nm). The prepared sample was then transferred to a N_2-filled glove box, and a solution of polythieno[3,4-*b*]-thiophene-*co*-benzodithiophene (PTB7) : [6,6]-phenyl C71 butyric acid methyl ester (PC71BM) (1 : 1.5, w/w) in chlorobenzene/1,8-diiodooctane (97 : 3, v/v) was spin-coated to form the photoactive layer (80 nm). Finally, MoO_3 (5 nm) and Ag anodes (100 nm) were sequentially deposited by thermal evaporation in a high-vacuum chamber ($<10^{-7}$ Torr). The active area of the fabricated inverted PSC was 4 mm^2.

Measurements

The thickness of the prepared thin film was measured using an Alpha step 500 surface profiler (KLA-Tencor) and AFM (PSIA XE-100, contact mode). The surface morphologies of the electron transport and photoactive layers were characterized by AFM (PSIA XE-100, non-contact mode). The energy levels of the ZnO and ZnO–PFN interlayers were measured using UV-Vis spectroscopy (Agilent 8453) and UPS (AXIS Ultra DLD, He I, $h\nu$ = 21.2 eV), and the surface tension was measured using a KRUSS K6 tensiometer. In addition, XPS (Thermo Electron, K-Alpha) and XRD (Bruker-AXS) were used to investigate the surface composition and lattice structure of the interlayer.

The current density–voltage (*J*–*V*) characteristics of the fabricated inverted PSCs were assessed using a Keithley 2400 source measure unit and an AM 1.5G solar simulator (Oriel 96000 150 W solar simulator). The incident photon-to-current conversion (IPCE) was measured to determine the best performance of the inverted devices. The electron mobility in the electron-only devices was assessed using the SCLC method.

Results and discussion

Fig. 1 shows the molecular structures of the donor within the photoactive layer (PTB7), the acceptor ($PC_{71}BM$), and the water/alcohol soluble conjugated polymer (PFN). As shown in the structure of the inverted device (Fig. 1d), PTB7 and $PC_{71}BM$ were incorporated into the bulk heterojunction structure in the photoactive layer. PFN was added to the ZnO solution and spin-coated as a single layer to form the ZnO–PFN interlayer.

As shown in Fig. 1e and f, the contact angles of the ZnO and ZnO–PFN-based electron extraction interlayers were 47.5° and 89.4°, respectively, when measured with deionized water, showing a lower wettability on the surface of the latter. In addition, the surface energy (23.9 mJ m^{-2}) was lower in the ZnO–PFN layer than that (50.2 mJ m^{-2}) of the ZnO layer. This result indicated that the surface characteristic of the ZnO film changed from hydrophilic to hydrophobic due to the addition of PFN and that a hydrophobic surface and a photoactive layer could come in close contact when they were sandwiched.[1] Moreover, PCBM and the surface of the ZnO–PFN film shared a similar surface energy of 22.5 mJ m^{-2},[3] allowing for the formation of a PCBM-rich phase in

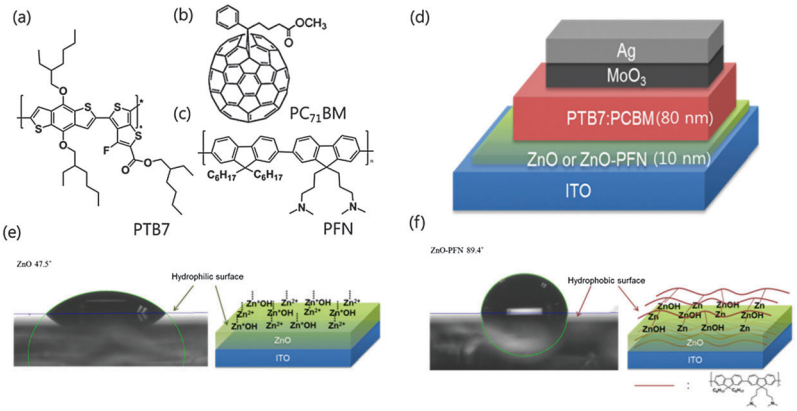

Fig. 1 Chemical structure of (a) PTB7, (b) PC71BM, (c) PFN and (d) a scheme of the inverted PSC device structure. The contact angle images by dropping DI water on the substrate and schemes for surface of (e) ITO/ZnO and (f) ITO/ZnO–PFN.

close contact with the ZnO–PFN layer in the bulk heterojunction (BHJ) film. As a result, electron transfer was accelerated by the close contact of the two layers and the photovoltaic device performance could be improved, accordingly.[1,2]

Fig. 2 shows changes in the chemical bonding and composition of the ZnO-only and ZnO–PFN interlayers based on XPS surface analysis. As shown in Fig. 2a, the carbon C 1s peak appeared at 285.7 eV on the surface of the ZnO–PFN layer, confirming the aromatic hydrocarbon molecules of PFN contained on the layer. This result was in agreement with the other findings of a higher contact angle value and lower surface energy described in Fig. 1e and f. In addition, the N 1s spectrum of the ZnO–PFN film displayed an additional peak at 400.6 eV, whereas the peak was not observed in the ZnO film, as shown in Fig. 2b. The peak at 400.6 eV observed on the ZnO–PFN film indicated $-N^{+}-$, suggesting bonding between the amine molecules of PFN and the zinc core. This finding was also confirmed in the spectra of zinc Zn 2p and oxygen O 1s, as shown in Fig. 2c and d.

In Fig. 2c, the Zn $2p_{3/2}$ peak corresponded to the Zn–O bond.[2] The Zn $2p_{3/2}$ peak in the ZnO–PFN surface appeared at 1021.8 eV, and its intensity was lower than that of the ZnO-only film at 1021.9 eV, indicating that the bonding of Zn–O was decreased due to $-N^{+}-$ that resulted from the bonding between the amine molecules of PFN and the zinc core.[31] In Fig. 2d, the O 1s spectra displayed three peaks at the binding energies of 530, 531.5 and 532.5 eV. The first two peaks corresponded to the oxygen that constituted stoichiometric ZnO and $Zn(OH)_2$ structures. The third peak at 532.5 eV corresponded to the bonding of the surface absorbed oxygen atoms with exposed dangling bonds in ZnO. The atomic concentration of oxygen on the ZnO–PFN surface was 49.6% and 41.8% at 530 and 531.5 eV, respectively, showing 0.3% and 1.9% increases from the atomic concentration levels of the ZnO film. However, the atomic concentration of oxygen decreased by 2.2% (10.8% to 8.6%) at 532.5 eV compared with the atomic concentration level of the ZnO film. This result indicated that the bonding between amine molecules and the zinc core led to a reduction in the oxygen deficiency in the surface concentration of hydroxyl groups and dangling bonds[2,32] and that PFN was effective at improving the surface properties of ZnO, as shown in Fig. 1e and f, *i.e.*, the surface energy was effectively modified in the ZnO–PFN layer to reduce surface defects.

As shown in Fig. S1 (ESI†), the X-ray diffraction patterns of interlayers can be assigned to the ZnO wurzite phase.[33,34] The X-ray diffraction peaks for ZnO–PFN film showed lower intensity than those of ZnO film without shift. It indicates that crystallite size of ZnO was decreased, maintaining ZnO wurzite phase, by adding PFN polymer.

Fig. 3a shows the UPS data of the ZnO and ZnO–PFN films at the secondary electron cutoff edge (E_{cutoff}) of 17.47 and 17.56 eV, respectively. Fig. 3b shows the UPS data of the two films at the valence region (E_{onset}) of 3.55 eV. Fig. 3c shows the UV-vis absorption spectra of the electron extraction layers. The inset data is the UV-vis absorption spectra of PFN, ZnO and ZnO–PFN film ($\sim$10 nm) without normalization. Only the ZnO–PFN film exhibited an absorption peak attributed to the π–π^* transition of PFN with λ_{max} = 388 nm. The band gap energies were calculated as 3.42 and 2.93 eV, respectively. The valence band of the ZnO and ZnO–PFN layers were calculated using the following equation:[1,2]

$$\text{V.B.}_{ETL} = h\nu - (E_{cutoff} - E_{onset})$$

The valence band in the ZnO and ZnO–PFN layers were 7.28 and 7.19 eV, respectively. The conduction band of the two layers was also calculated using the valence band and band gap energies and presented in the energy diagram in Fig. 3d. The conduction band of the ZnO–PFN layer was lowered from 3.86 to 4.26 as a result of the addition of PFN. These results demonstrated a reduction in ZnO defects and strong dipole formation at the interface between ZnO and PFN.[2,35] The lowered energy level also implied the formation of a new pathway for electron transfer in the photoactive layer.

Fig. 4 shows the current density (J)–voltage (V) curve and incident photon to current conversion efficiency (IPCE) data in the inverted PSC devices. The photovoltaic performance of the devices is summarized in Table 1.[36] The device with the ZnO electron extraction layer showed short circuit current

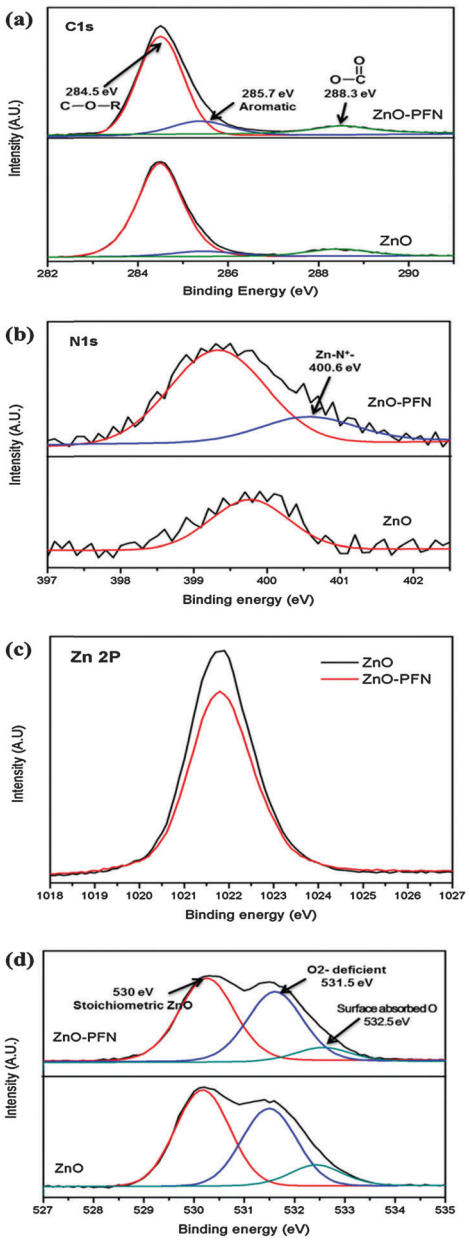

Fig. 2 XPS analysis on ITO/ZnO and ITO/ZnO–PFN for (a) carbon C 1s, (b) nitrogen N 1s, (c) zinc Zn $2p_{3/2}$, and (d) oxygen O 1s.

(J_{sc}) = 16.3 mA cm^{-2}, open circuit voltage (V_{oc}) = 0.717 V, fill factor (FF) = 64.7% and PCE = 7.2%. The device with the ZnO–PFN interlayer showed J_{sc} = 18.3 mA cm^{-2}, V_{oc} = 0.737 V, FF = 67.8% and PCE = 9.2%. The calculated J_{sc} values from IPCE data were 14.4 and 16.0 mA cm^{-2}. The inconsistency between IPCE and J_{sc} values was attributed to the different spectral-mismatch factors of different light sources.[37,38] Thus, the PFN material could boost the PCE as high as 28% by increasing the J_{sc} and FF. In other words, a lowered surface energy and tuned energy levels provided a better interface between the photo-active and ZnO–PFN electron-extracting layers.

Fig. 5a and b show that the surface RMS roughness was 2.483 nm in the ZnO–PFN layer and 2.176 nm in the ZnO layer.

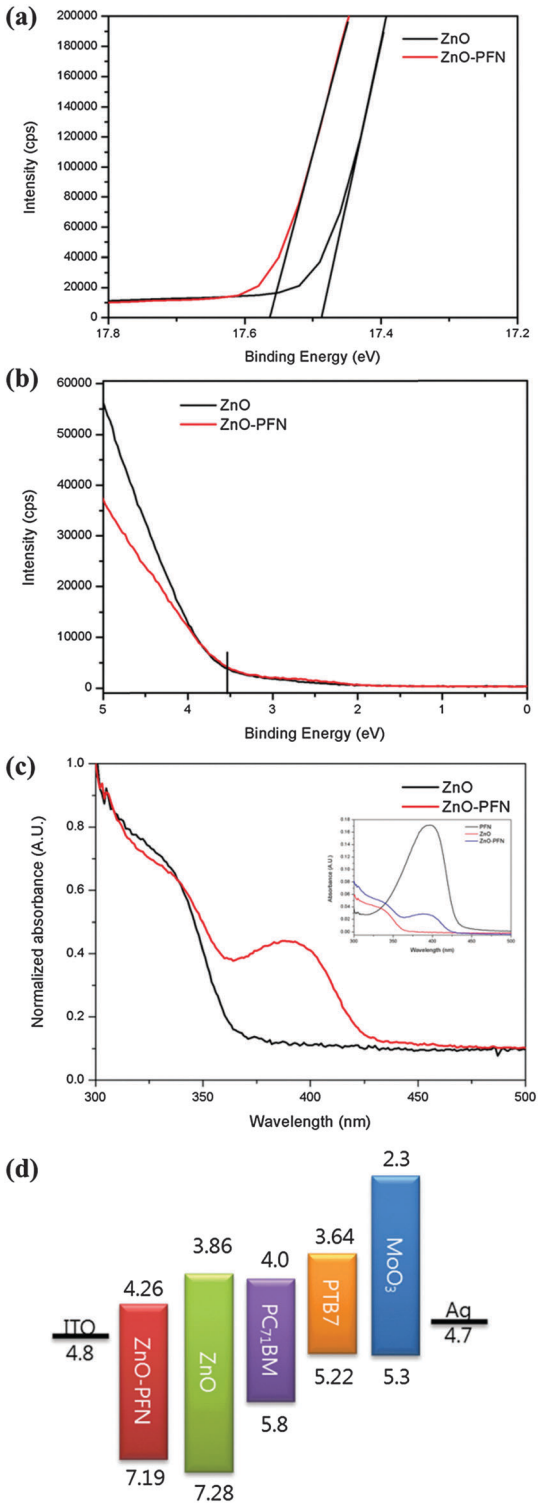

Fig. 3 UPS spectra of ZnO or ZnO–PFN coated on ITO substrate: (a) secondary electron cutoff, (b) valence region, (c) UV-Vis spectrum of ZnO or ZnO–PFN and (d) energy diagram of the inverted devices.

The rougher surface in the ZnO–PFN layer was associated with a higher density array of vertically aligned nanopillars.[16,39] High surface roughness along with high density array of vertical nanopillars facilitated the transport of the electrons, which

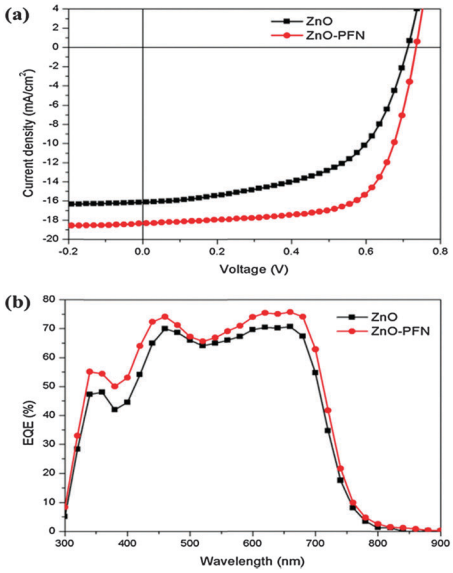

Fig. 4 (a) J–V characteristics and (b) external quantum efficiency (EQE) characteristics of PSCs.

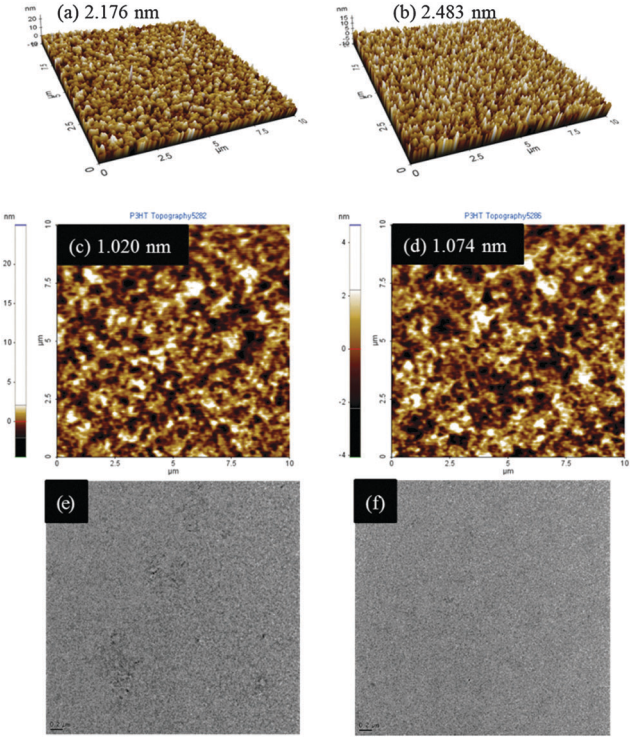

Fig. 5 AFM images of (a) ZnO, (b) ZnO–PFN, (c) ZnO/PTB7:PCBM, and (d) ZnO–PFN/PTB7:PCBM, inset is the RMS roughness. TEM images of (e) ZnO/PTB7:PCBM and (f) ZnO–PFN/PTB7:PCBM.

were separated from the photoactive layer, toward the cathode, creating a large interfacial area between the ZnO–PFN layer and the photoactive layer.[16,39] Fig. 5c and d show the AFM topology images of the PTB7:PCBM photoactive layer deposited on top of the electron extraction layer. In comparison with the RMS roughness shown in Fig. 5a and b, the difference in the photoactive layer was less significant. As shown in the TEM and AFM phase images (Fig. 5e and f and Fig. S2, ESI†), greater homogeneity and phase separation were observed in the photoactive layer deposited on top of the ZnO–PFN interlayer.

To identify the effects of the changes in the surface properties and energy levels of the ZnO–PFN interlayer on electron transfer, the electron mobility in the electron-only devices was measured using the Mott–Gurney space charge limited current (SCLC) formula[1,40] given as follows:

$$J = (9/8)\mu e\varepsilon_0\varepsilon r(V^2/L^3)$$

The electron transport *via* the interlayers was measured in the devices with ITO/ZnO or ZnO–PFN/Al electrons, and the electron mobility of the photoactive layer was also measured in the devices with ITO/ZnO or ZnO–PFN/PTB7:PCBM/Al (Fig. S3, ESI†). The measured values of electron mobility are summarized in Table S1 (ESI†). It is found that the ITO/ZnO or ZnO–PFN/Al devices show perfectly linear lines, which are characteristic of a true Ohmic contact between interlayers and electrode interfaces.[41,42] The inverse of the slope can represent the resistance of interlayers.[43] The series resistance of solar cells has a similar trend with the ETL resistance obtained from the J–V curve. The electron mobility of the photoactive layer was calculated using the SCLC formula. The values were 1.71×10^{-4} and 6.60×10^{-4} $cm^2\ V^{-1}\ s^{-1}$ showing about a four times increase in the ZnO–PFN interlayer based device. The improved electron mobility was attributed to the large interfacial area between the photoactive layer and the interlayer, reduced series resistance and increased shunt resistance through energy level alignment and reduced recombination of electron holes within the devices. Therefore, electrons could effectively move from the photoactive layer to the cathodes and exit the device, leading to the increase in the J_{sc}, FF and eventually the PCE.

A device long-term stability test was performed by storing the devices in a N_2-filled glove box. The time-dependent decline in PCE is shown in Fig. 6. The ZnO-based device maintained a

Table 1 Photovoltaic performances of inverted PSCs

Cathode		J_{sc} [mA cm^{-2}]	V_{oc} [V]	FF [%]	PCE [%]	Cal. J_{sc} [mA cm^{-2}]	R_s [Ω cm^2]	R_{sh} [Ω cm^2]
ITO/ZnO	Best	16.3	0.717	61.7	7.2	14.4	6.5	714
	Ave.	16.0 ± 0.3	0.717	61 ± 2.5	6.9 ± 0.3		—	—
ITO/ZnO–PFN	Best	18.3	0.737	67.8	9.2	16.0	5.3	990
	Ave.	18.3 ± 0.3	0.737	66.0 ± 2.5	8.95 ± 0.25		—	—
Conventional structure[a]		14.9	0.737	60.7	6.6		8.0	835

[a] Conventional structure:[36] ITO/PEDOT:PSS/PTB7:PCBM/PFN/Al. The average values and deviations were obtained from ten devices.

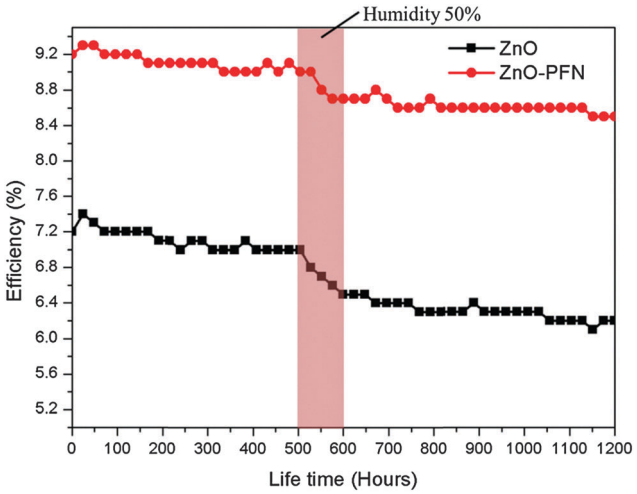

Fig. 6 Power conversion efficiency variation of the devices with time stored in a N_2 filled glovebox.

PCE of 6.2%, whereas the ZnO–PFN based device maintained a PCE of 8.5%. To determine the effects of humidity on efficiency decrease, the time-dependent decline in the PCE was measured at 25 °C and a humidity of 50% for 100 hours after the initial 500 hours. During 100 hours, the ZnO–PFN based device showed a 3.3% efficiency decrease, whereas the ZnO-based device showed a 7.2% efficiency decrease. The findings revealed a contribution of the ZnO–PFN interlayer to the long-term stability of the inverted solar cells. The reproducibility of the devices was assessed by creating ten devices, and the results are presented in Fig. S4 (ESI†). The V_{oc} values of all the devices were same at 0.737 V, and the PCE was 8.95% with a J_{sc} value of 18.3 mA cm^{-2} and a FF value of 66% on average.

Conclusions

A ZnO–PFN interlayer was introduced to improve the efficiency and stability of inverted PSCs. The ZnO/PFN hybrid interlayer with a hydrophobic surface was deposited on top of the ITO electrode and the ZnO surface defects were reduced through the modification of the chemical composition. In addition, the interfacial area between the photoactive layer and the electron extraction layer was increased through energy level tuning and subsequent improvement in electron extraction. As a result, the PCE of the device fabricated with ZnO–PFN increased up to 9.2%, along with improvement in the stability. The ZnO–PFN interlayer aimed to overcome the drawbacks of the conventional hydrophilic surface of ZnO based on the properties of the conjugated polymer (PFN) without additional requirements. It was therefore simple to fabricate the inverted PSCs, making the devices commercially viable. At the same time, the high PCE ensured high device performance.

Acknowledgements

This study was supported by the New & Renewable Energy Core Technology Program of the Korea Institute of Energy Technology Evaluation and Planning (KETEP), granted financial resource from the Ministry of Trade, Industry & Energy, Republic of Korea (No. 20133030000180) and by the National Research Foundation of Korea Grant funded by the Korean Government (MEST) (NRF-2009-C1AAA001-2009-0093526).

References

1 S.-H. Liao, H.-J. Jhuo, Y.-S. Cheng and S.-A. Chen, *Adv. Mater.*, 2013, **25**, 4766–4771.
2 K. Yuan, L. Chen, F. Li and Y. Chen, *J. Mater. Chem. C*, 2014, **2**, 1018–1027.
3 S. W. Heo, K. W. Song, M. H. Choi, H. S. Oh and D. K. Moon, *Sol. Energy Mater. Sol. Cells*, 2013, **114**, 82–88.
4 S. W. Heo, S. H. Kim, E. J. Lee and D. K. Moon, *Sol. Energy Mater. Sol. Cells*, 2013, **111**, 16–22.
5 S. W. Heo, K. H. Baek, H. J. Song, T. H. Lee and D. K. Moon, *Macromol. Mater. Eng.*, 2014, **299**, 353–360.
6 S. J. Lou, J. M. Szarko, T. Xu, L. Yu, T. J. Marks and L. X. Chen, *J. Am. Chem. Soc.*, 2011, **133**, 20661–20663.
7 C. H. Y. Ho, Q. Dong, H. Yin, W. W. K. Leung, Q. Yang, H. K. H. Lee, S. W. Tsang and S. K. So, *Adv. Mater. Interfaces*, 2015, **2**, 1500166.
8 Y. Zhu, X. Xu, L. Zhang, J. Chen and Y. Cao, *Sol. Energy Mater. Sol. Cells*, 2012, **97**, 83–88.
9 S. W. Heo, K. W. Song and D. K. Moon, *RSC Adv.*, 2014, **4**, 6776–6781.
10 Z. He, C. Zhong, X. Huang, W.-Y. Wong, H. Wu, L. Chen, S. Su and Y. Cao, *Adv. Mater.*, 2011, **23**, 4636–4643.
11 S. Kim, J. H. Koh, X. Yang, W. S. Chi, C. Park, J. W. Leem, B. Kim, S. Seo, Y. Kim, J. S. Yu, J. H. Kim and E. Kim, *Adv. Energy Mater.*, 2014, **4**, 1301338.
12 S. Guo, B. Cao, W. Wang, J.-F. Moulin and P. Müller-Buschbaum, *ACS Appl. Mater. Interfaces*, 2015, **7**, 4641–4649.
13 H. Zhou, Y. Zhang, J. Seifter, S. D. Collins, C. Luo, G. C. Bazan, T. Q. Nguyen and A. J. Heeger, *Adv. Mater.*, 2013, **25**, 1646–1652.
14 S. Guo, J. Ning, V. Körstgens, Y. Yao, E. M. Herzig, S. V. Roth and P. Müller-Buschbaum, *Adv. Energy Mater.*, 2015, **5**, 1401315.
15 Z. He, C. Zhong, S. Su, M. Xu, H. Wu and Y. Cao, *Nat. Photonics*, 2012, **6**, 591–595.
16 Z. Yin, Q. Zheng, S.-C. Chen, D. Cai, L. Zhou and J. Zhang, *Adv. Energy Mater.*, 2014, **4**, 1301404.
17 S. R. Dupont, E. Voroshazi, D. Nordlund, K. Vandewal and R. H. Dauskardt, *Adv. Mater. Interfaces*, 2014, **1**, 1400135.
18 P. Cheng, J. Hou, Y. Li and X. Zhan, *Adv. Energy Mater.*, 2014, **4**, 1301349.
19 Y.-M. Chang and C.-Y. Leu, *J. Mater. Chem. A*, 2013, **1**, 6446–6451.
20 K. Sun, H. Zhang and J. Ouyang, *J. Mater. Chem.*, 2011, **21**, 18339–18346.
21 C.-H. Hsieh, Y.-J. Cheng, P.-J. Li, C.-H. Chen, M. Dubosc, R.-M. Liang and C.-S. Hsu, *J. Am. Chem. Soc.*, 2010, **132**, 4887–4893.

22 O. Pachoumi, A. A. Bakulin, A. Sadhanala, H. Sirringhaus, R. H. Friend and Y. Vaynzof, *J. Phys. Chem. C*, 2014, **118**, 18945–18950.
23 A. K. K. Kyaw, D. H. Wang, V. Gupta, J. Zhang, S. Chand, G. C. Bazan and A. J. Heeger, *Adv. Mater.*, 2013, **25**, 2397–2402.
24 T. Yang, M. Wang, C. Duan, X. Hu, L. Huang, J. Peng, F. Huang and X. Gong, *Energy Environ. Sci.*, 2012, **5**, 8208–8214.
25 S. K. Hau, Y.-J. Cheng, H.-L. Yip, Y. Zhang, H. Ma and A. K. Y. Jen, *ACS Appl. Mater. Interfaces*, 2010, **2**, 1892–1902.
26 Y.-J. Cheng, C.-H. Hsieh, Y. He, C.-S. Hsu and Y. Li, *J. Am. Chem. Soc.*, 2010, **132**, 17381–17383.
27 C.-Y. Chang, C.-E. Wu, S.-Y. Chen, C. Cui, Y.-J. Cheng, C.-S. Hsu, Y.-L. Wang and Y. Li, *Angew. Chem., Int. Ed.*, 2011, **50**, 9386–9390.
28 J.-D. Chen, L. Zhou, Q.-D. Ou, Y.-Q. Li, S. Shen, S.-T. Lee and J.-X. Tang, *Adv. Energy Mater.*, 2014, **4**, 1301777.
29 C. Xu and Z. L. Wang, *Adv. Mater.*, 2011, **23**, 873–877.
30 S. Xue, L. Yao, F. Shen, C. Gu, H. Wu and Y. Ma, *Adv. Funct. Mater.*, 2012, **22**, 1092–1097.
31 M. Navaneethan, J. Archana, M. Arivanandhan and Y. Hayakawa, *Chem. Eng. J.*, 2012, **213**, 70–77.
32 T. Rakshit, S. P. Mondal, I. Manna and S. K. Ray, *ACS Appl. Mater. Interfaces*, 2012, **4**, 6085–6095.
33 Y. W. Chen, Y. C. Liu, S. X. Lu, C. S. Xu, C. L. Shao, C. Wang, J. Y. Zhang, Y. M. Lu, D. Z. Shen and X. W. Fan, *J. Chem. Phys.*, 2005, **123**, 134701.
34 O. Game, U. Singh, A. A. Gupta, A. Suryawanshi, A. Banpurkar and S. Ogale, *J. Mater. Chem.*, 2012, **22**, 17302.
35 K.-D. Kim, D. C. Lim, J. Hu, J.-D. Kwon, M.-G. Jeong, H. O. Seo, J. Y. Lee, K.-Y. Jang, J.-H. Lim, K. H. Lee, Y. Jeong, Y. D. Kim and S. Cho, *ACS Appl. Mater. Interfaces*, 2013, **5**, 8718–8723.
36 H. J. Song, E. J. Lee, D. H. Kim, T. H. Lee, M. Goh, S. Lee and D. K. Moon, *Dyes Pigm.*, 2015, **113**, 210–218.
37 P. Schilinsky, C. Waldauf and C. J. Brabec, *Adv. Funct. Mater.*, 2006, **16**, 1669–1672.
38 Y. H. Chang, S. R. Tseng, C. Y. Chen, H. F. Meng, E. C. Chen, S. F. Horng and C. S. Hsu, *Org. Electron.*, 2009, **10**, 741.,
39 T. Earmme and S. A. Jenekhe, *J. Mater. Chem.*, 2012, **22**, 4660–4668.
40 H. T. Nicolai, G. A. H. Wetzelaer, M. Kuik, A. J. Kronemeijer, B. de Boer and P. W. M. Blom, *Appl. Phys. Lett.*, 2010, **96**, 172107.
41 X. D. Feng, C. J. Huang, V. Lui, R. S. Khangura and Z. H. Lu, *Appl. Phys. Lett.*, 2005, **86**, 143511.
42 J. S. Park, J. M. Lee, S. K. Hwang, S. H. Lee, H.-J. Lee, B. R. Lee, H. Il Park, J.-S. Kim, S. Yoo, M. H. Song and S. O. Kim, *J. Mater. Chem.*, 2012, **22**, 12695.
43 J.-L. Lan, Z. Liang, Y.-H. Yang, F. S. Ohuchi, S. A. Jenekhe and G. Cao, *Nano Energy*, 2014, **4**, 140–149.